Technical Review

No. 1 – 1996

Calibration Uncertainties & Distortion of Microphones.
Wide Band Intensity Probe. Accelerometer Mounted Resonance Test

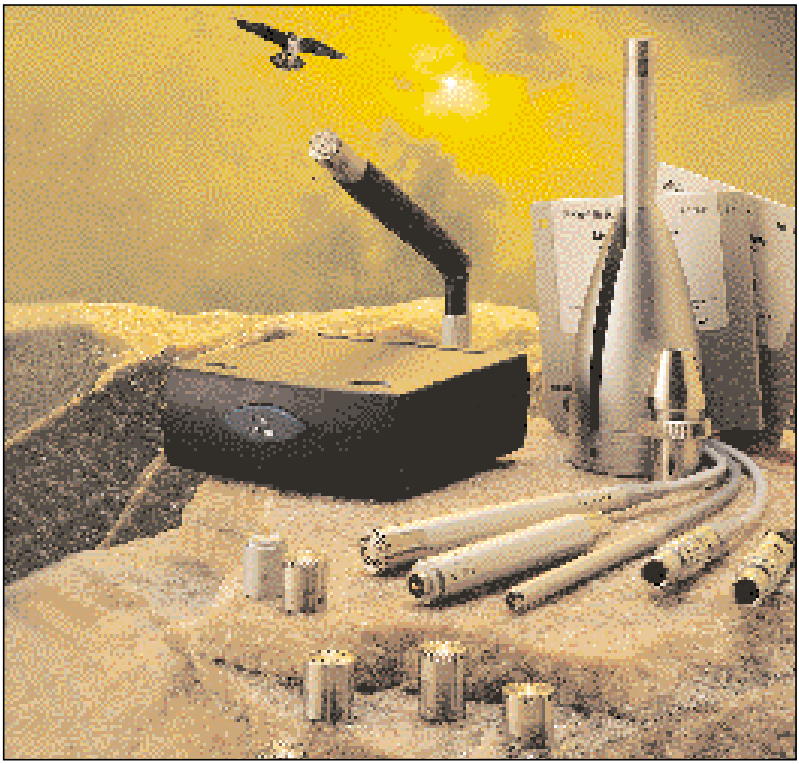

Brüel & Kjær

Previously issued numbers of Brüel & Kjær Technical Review

2 – 1995 Order Tracking Analysis
1 – 1995 Use of Spatial Transformation of Sound Fields (STSF) Techniques in the Automotive Industry
2 – 1994 The use of Impulse Response Function for Modal Parameter Estimation
Complex Modulus and Damping Measurements using Resonant and Non-resonant Methods (Damping Part II)
1 – 1994 Digital Filter Techniques vs. FFT Techniques for Damping Measurements (Damping Part I)
2 – 1990 Optical Filters and their Use with the Type 1302 & Type 1306 Photoacoustic Gas Monitors
1 – 1990 The Brüel & Kjær Photoacoustic Transducer System and its Physical Properties
2 – 1989 STSF — Practical instrumentation and application
Digital Filter Analysis: Real-time and Non Real-time Performance
1 – 1989 STSF — A Unique Technique for scan based Near-Field Acoustic Holography without restrictions on coherence
2 – 1988 Quantifying Draught Risk
1 – 1988 Using Experimental Modal Analysis to Simulate Structural Dynamic Modifications
Use of Operational Deflection Shapes for Noise Control of Discrete Tones
4 – 1987 Windows to FFT Analysis (Part II)
Acoustic Calibrator for Intensity Measurement Systems
3 – 1987 Windows to FFT Analysis (Part I)
2 – 1987 Recent Developments in Accelerometer Design
Trends in Accelerometer Calibration
1 – 1987 Vibration Monitoring of Machines
4 – 1986 Field Measurements of Sound Insulation with a Battery-Operated Intensity Analyzer
Pressure Microphones for Intensity Measurements with Significantly Improved Phase Properties
Measurement of Acoustical Distance between Intensity Probe Microphones
Wind and Turbulence Noise of Turbulence Screen, Nose Cone and Sound Intensity Probe with Wind Screen
3 – 1986 A Method of Determining the Modal Frequencies of Structures with Coupled Modes
Improvement to Monoreference Modal Data by Adding an Oblique Degree of Freedom for the Reference
2 – 1986 Quality in Spectral Match of Photometric Transducers
Guide to Lighting of Urban Areas

(Continued on cover page 3)

Technical Review

No.1 – 1996

Contents

Copyright © 1994, Brüel & Kjær A/S
All rights reserved. No part of this publication may be reproduced or distributed in any form, or by any means, without prior written permission of the publishers. For details, contact:
Brüel & Kjær A/S, DK-2850 Nærum, Denmark.

Editor: Harry K. Zaveri
Layout: Judith Sarup
Photographer: Peder Dalmo
Printed by Nærum Offset

A Sound Intensity Probe for Measuring from 50 Hz To 10 kHz

by F. Jacobsen, V. Cutanda) and P. M. Juhl, Department of Acoustic Technology, Technical University of Denmark, Building 352, DK-2800 Lyngby, Denmark*

Abstract

The upper frequency limit of a p-p sound intensity probe with a certain microphone separation distance is generally considered to be the frequency at which an ideal probe would exhibit an acceptably small finite difference error in a plane wave of axial incidence. This article shows that the resonances of the cavities in front of the microphones in the usual 'face-to-face' configuration give rise to a pressure increase that to some extent compensates for the finite difference error. Thus the operational frequency range can be extended to an octave above the limit determined by the finite difference error, if the length of the spacer between the microphones equals the diameter.

Résumé

Pour une sonde d'intensité acoustique à deux microphones séparés par une distance donnée, la limite supérieure de fréquence est généralement considérée comme la fréquence à laquelle une sonde idéale présenterait, pour une onde plane et une incidence de 0°, une erreur de différence finie acceptable. Cet article montre que le phénomène de résonance dû aux cavités frontales des microphones configurés "face à face" entraîne un accroissement de pression tendant à compenser cette erreur. La gamme de fréquence opérationnelle peut donc être élargie d'un octave au-dessus de la limite ainsi imposée, si le bloc d'espacement présente une longueur égale au diamètre.

*) Present address: U.P.M., E.U.I.T. de Telecomunicación, Department of Audiovisual Engineering and Communications, Ctra de Valencia km 7, E-28031 Madrid, Spain

Zusammenfassung

Die obere Grenzfrequenz einer Zwei-Mikrofon-Schallintensitätssonde mit einem bestimmten Mikrofonabstand wird allgemein als diejenige Frequenz betrachtet, bei der die ideale Sonde einen noch akzeptablen Fehler, bedingt durch den endlichen Abstand der beiden Mikrofone, für eine axial einfallende ebene Welle zeigt. Dieser Artikel zeigt, daß die Resonanzen der Hohlräume vor den Mikrofonen bei der üblichen Anordnung (Mikrofone einander gegenüber) einen Druckanstieg verursachen, der den Abstandsfehler teilweise kompensiert. Der Arbeitsfrequenzbereich kann daher auf eine Oktave über der durch den Abstandsfehler definierten Grenze erweitert werden, wenn die Länge des Mikrofonabstandstücks gleich dem Mikrofondurchmesser ist.

Introduction

Sound power determination is a central point in noise control engineering, and the method of sound power determination based on measurement of sound intensity has the significant advantage over other methods that it makes it possible to determine the sound power of a source of noise in situ, even in the presence of other sources.

Existing sound intensity probes in commercial production are based on the "two-microphone" (p-p) measurement principle in which the intensity is determined from the signals from two closely spaced pressure microphones.

One of the obvious limitations of this measurement principle is the frequency range; the fact that the method relies on the finite difference approximation clearly implies an upper frequency limit that is inversely proportional to the distance between the microphones. Unfortunately, the influence of phase mismatch and several other measurement errors is also inversely proportional to the distance between the microphones; therefore, one cannot extend the frequency range simply by placing the microphones very close together.

One can extend the frequency range by combining measurements with two sets of microphones. The purpose of this paper is to examine whether it is possible to cover a significant part of the audible frequency range, from 50 Hz to 10 kHz, with one single probe configuration.

Numerical Results

In what follows it is assumed that the intensity probe is a p-p probe with the two microphones in the usual 'face-to-face' arrangement with a solid 'spacer' between them.

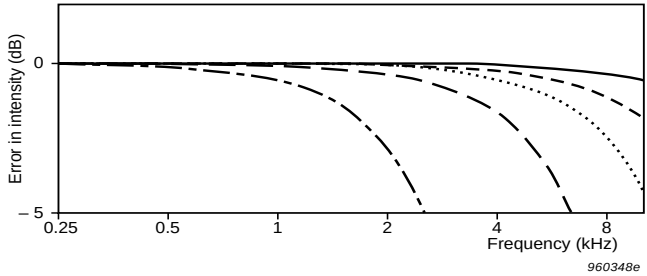

Fig. 1. Finite difference error of an ideal intensity probe which does not disturb the sound field in a plane wave of axial incidence for different values of the separation distance —, 5 mm; ---. 8.5 mm; ···, 12 mm; – –, 20 mm; – - – -, 50 mm

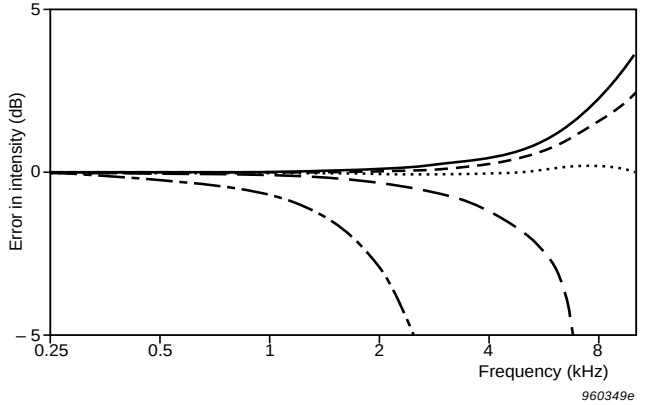

Fig. 2. Error of an intensity probe with 12 mm long half-inch microphones in a plane wave of axial incidence for different spacer lengths, —, 5 mm; ---, 8,5 mm; ···, 12 mm; – –, 20 mm; – - – -, 50 mm

The operational frequency range of an intensity probe depends on the particulars of the sound field conditions [1]. Nevertheless, the highest frequency at which an ideal p-p probe with a certain microphone separation distance would exhibit an acceptably small finite difference error in a plane wave of axial incidence has usually been regarded as the upper frequency limit [1]. This finite difference error is shown in Fig. 1. According to this reasoning a probe with half-inch microphones separated by a 12 mm spacer (which is a very common configuration) should not be used above, say, 5 kHz. However, more than ten years ago Watkinson and Fahy pointed out that the resonance of the cavities in front of the microphones in this configuration gives rise to a pressure increase that to some extent might compensate for the finite difference error [2] A recent investigation based on a boundary element model of an axisymmetric p-p probe has confirmed Watkinson and Fahy's observation [3]. Fig. 2, which corresponds to Fig. 1, shows the error calculated for a probe with two 12 mm long half-inch microphones. The error is essentially the result of the combined effect of the finite difference approximation and the pressure increase. It is

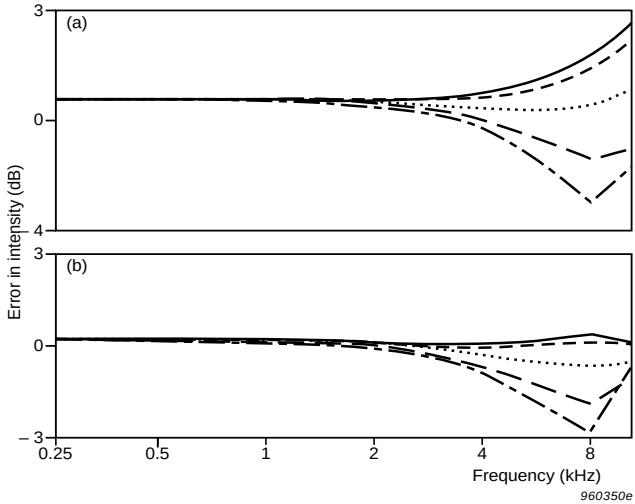

Fig. 3. Error of an intensity probe with 12 mm long half-inch microphones in a plane wave. (a) 8.5 mm spacer; (b) 12 mm spacer. Angle of incidence: —, 0°; ---, 20°; ···, 40°; – –, 60°; – - – -, 80°

apparent that the optimum length of the spacer is about 12 mm, and that a probe with this geometry performs very well in the case of a plane wave of axial incidence up to 10 kHz. It can also be deduced from the figure that such a probe is superior to a probe with quarter-inch microphones separated by a 12 mm spacer, owing to the fact that the compensating pressure increase is shifted an octave upwards for the latter configuration. In Fig. 3 is shown the corresponding error for non-axial incidence, calculated for two different spacer lengths.

Experimental Results

The numerical results briefly summarised in the foregoing imply that the frequency range of a probe with the conventional combination of half-inch microphones and a 12 mm spacer is wider than hitherto believed. To test this conclusion a series of experiments have been carried out: the sound power of a loudspeaker driven with pink noise, Brüel & Kjær Type 4205, was determined in a large ($240\,m^3$) reverberant room with a reverberation time of about 4 s. The source was placed on the floor about 1.5 m from the nearest wall, and the ratiated sound power was estimated by scanning manually with an intensity probe over the five faces of a cubic surface of $1 \times 1 \times 1$ m.

A frequency analyser of Brüel & Kjær Type 3550 was used in combination with an intensity probe of Brüel & Kjær Type 3548, either with half-inch microphones of Brüel & Kjær Type 4181 or with quarter-inch microphones of Brüel & Kjær Type 4178. Since these microphones are so-called free-field microphones it is necessary to compensate for the drop of the pressure sensitivity at high frequencies. Fig. 4 shows the pressure response of the two sets of microphones, determined with an electrostatic actuator. All the results presented in the following have been corrected with the corresponding actuator response.

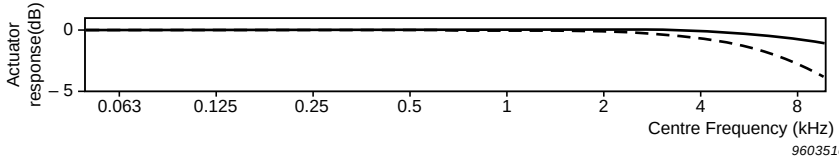

Fig. 4. Electrostatic actuator response of microphones. — , Brüel & Kjær Type 4178; --- , Brüel & Kjær Type 4181

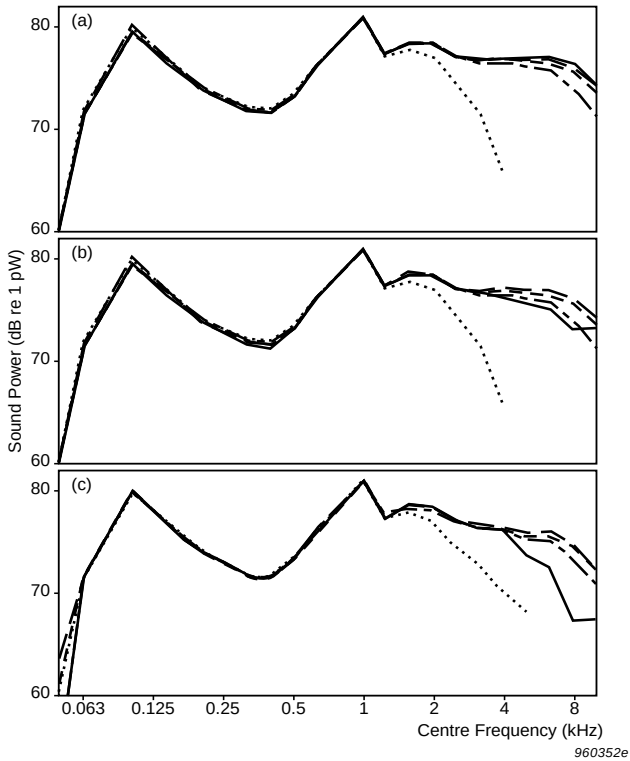

Fig. 5. Sound power of source, estimated with different combinations of microphones and spacers. (a) No extraneous noise, (b) strong diffuse background noise from an extraneous source, (c) strong diffuse and non-diffuse noise from an extraneous source. — , Half-inch microphones, 8.5 mm spacer; --- , half-inch microphones, 12 mm spacer; ··· , half-inch microphones, 50 mm spacer; – – , quarter-inch microphones, 6 mm spacer; – - – -, quarter-inch microphones, 12 mm spacer

The measurements were carried out under three conditions: i) without extraneous noise, ii) with strong diffuse background noise from a distant source (Airap A14 from Électricité de France), and iii) with strong non-diffuse and diffuse background noise from the same source placed about 2.5 m from the surface. In the last mentioned case the partial sound power of the nearest $1\,m^2$ segment was negative in the entire frequency range.

The measurements with quarter-inch microphones were carried out with a 6 mm spacer and with a 12 mm spacer. The former measurement, which can be expected to be reliable at high frequencies, served as the reference in the frequency range from 4 to 10 kHz. The measurements with half-inch microphones were carried out with an 8.5 mm spacer, a 12 mm spacer and a 50 mm spacer. In order to reduce the effect of transducer phase mismatch as far as possible, all measurements were repeated with the two microphones interchanged [4].

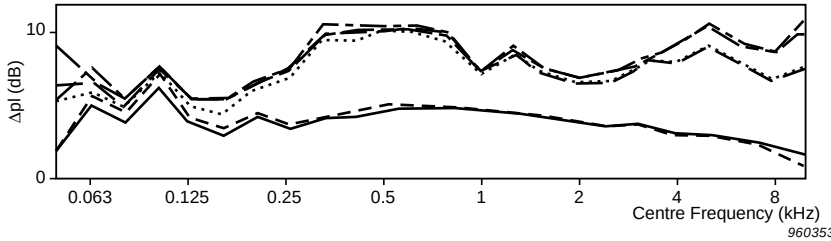

Fig. 6. Pressure-intensity index. —, Quarter-inch microphones, 6 mm spacer, no extraneous noise; ---, half-inch microphones, 12 mm spacer, no extraneous noise, ···, quarter-inch microphones, 6 mm spacer, diffuse noise; – –, half-inch microphones, 12 spacer, diffuse noise; – · –. quarter-inch microphones 6 mm spacer, non-diffuse and diffuse noise: – - – -, half-inch microphones, 12 mm spacer, non diffuse and diffuse noise

The results of the sound power measurements are presented in Fig. 5; and Fig. 6, which shows the pressure-intensity index, gives an impression of the acoustic conditions. It can be seen from Fig. 5 that practically all measurements are in agreement from 50 Hz to 1.25 kHz. An exception is the measurements with quarter-inch microphones at 50 Hz under the most difficult sound field condition. (This is probably the result of random errors due to electrical noise [5]; however, without compensation for phase mismatch significant errors occurred with the quarter-inch microphones in most of the frequency range.) From 1.6 kHz and upwards the combination of half-inch microphones and the 50 mm spacer underestimates, but it is worth noting that the error is less than predicted by the idealised expression for an axial plane wave (Fig. 1), and that the size of the error depends on the sound field conditions, which leads to the conclusion that one cannot compensate for the finite difference error. The combination of quarter-inch microphones and a 12 mm spacer leads to underestimation from 5 kHz and upwards, more or less as expected. The

measurements with half-inch microphones and the 12 mm spacer are in fair agreement with the reference measurements, confirming the predicted advantage of this combination. In fact, only the combination of half-inch microphones and the 8.5 mm spacer behaves unexpectedly.

As can be seen, it overestimates slightly under mild measurement conditions, but underestimates under more difficult conditions. It seems as if the ability of suppressing extraneous noise at high frequencies deteriorates if the spacer is significantly shorter than the diameter of the microphones. A possible explanation is that the error depends more on the angle of incidence for this configuration, cf. Fig. 3.

Conclusions

One cannot compensate for the finite difference error of p-p intensity probes by using the theoretical plane wave expression, and one cannot extend the frequency range by using a spacer appreciately shorter than the diameter of the microphones. Moreover, existing quarter-inch microphones are not suitable for measurement of sound intensity at low frequencies. However, a numerical and experimental study of diffraction effects has demonstrated that the operational frequency range can be extended to an octave above the limit determined by the finite difference error if the length of the spacer between the microphones equals the diameter. This means that a probe with half-inch microphones can cover the frequency range from 50 Hz to 10 kHz.

References

[1] FAHY, F.J.: "*Sound Intensity*" (E & FN Spon (second ed.), London 1995)

[2] WATKINSON, P.S.: and FAHY, F.J.:J. Sound Vib. 94, 299-306 (1984)

[3] CUTANDA, V.: JUHL P.M. and JACOBSEN, F. : "*A numerical investigation of the performance of sound intensity probes at high frequencies*" Proc. Fourth Int. Congress on Sound and Vib., 1996, pp. 1897 – 1904

[4] REN, M.: and JACOBSEN, F.: Noise Control Eng. J. 38, 17-25 (1992)

[5] JACOBSEN, F.: J. Sound Vib. 166, 195-207 (1993)

Measurement of Microphone Free-field Corrections and Determination of their Uncertainties

by Erling Frederiksen and Johan Gramtorp

Abstract
Modern measurement techniques and international cooperation on calibration research have made it possible to obtain more accurate free-field and diffuse-field corrections. In this article the methods and measurements are described and calculations of the uncertainties for the free-field corrections for microphone Type 4191 (12.5 mV/Pa) are shown.

Résumé
Les techniques de mesure modernes et la coopération internationale dans la recherche sur le calibrage ont contribué à améliorer la précision des corrections de champ libre et de champ diffus. Cet article décrit les différentes méthodes de mesure utilisées et présente un calcul d'incertitude pour les corrections champ libre du Microphone Type 4191 (12.5mV/Pa).

Zusammenfassung
Moderne Meßtechnik und internationale Zusammenarbeit auf dem Gebiet der Kalibrierung ermöglichen eine höhere Präzision bei Freifeld- und Diffusfeldkorrekturen. Dieser Artikel beschreibt die verschiedenen Meßmethoden sowie die Berechnung der Unsicherheit der Freifeldkorrektur für das Mikrofon Typ 4191 (12,5 mV/Pa).

Introduction
The most commonly used method for frequency response calibration of measurement microphones is still to measure the individual electrostatic actuator response and to add corrections to this. The corrections are the same for all microphones of the same type. For well-documented microphone types, free-field

and diffuse-field corrections are available from the microphone manufacturers. Brüel & Kjær has recently developed a new line of 1/2″ microphone types (Falcon Range) and has determined their corrections which are to be used for calibration at the factory and at calibration service laboratories abroad.

The principles applied for the determination of these free-field and diffuse-field corrections are the same as those used in the past but modern measurement techniques and international co-operation on calibration research have significantly improved the possibilities for obtaining more accurate corrections. Today, many countries and companies are improving their calibration systems. Therefore, there is an increasing demand for accurate corrections with documented uncertainty. The methods, the measurements and the uncertainties related to the resulting corrections for Type 4191 (12.5 mV/Pa) are discussed in this article.

Description of Free-field and Diffuse-field Corrections

The free-field correction is the ratio between the free-field response and the response of the microphone diaphragm system, Fig. 1. The correction is dominantly determined by sound reflection and refraction caused by the microphone body. There are two different types of free-field corrections. They refer

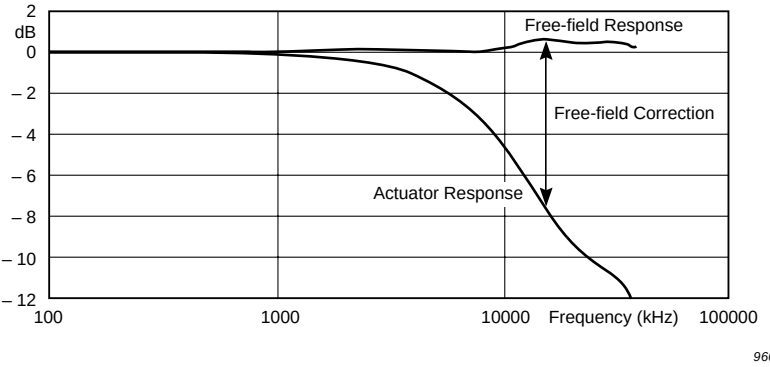

Fig. 1. Free-field Frequency Response of a Type 4191 microphone obtained by adding the Free-field Correction to an individually measured Actuator Response

to the slightly different pressure and actuator responses. Both responses account for the individual properties of the microphone diaphragm systems. They are relatively easy to measure in comparison with the free-field response. Actuator response calibrations are especially simple and require no special acoustic facilities. The Diffuse-field Response can be determined in the same way by applying other corrections to the actuator response.

Free-field Response Measurement

Three microphones were calibrated together. Pair-wise they were mounted in an anechoic room where one was transmitting sound to another. Microphone (a) transmitted to receiver (b), (b) to (c) and (c) to (a).

In order to minimise the influence of room reflections a rather large room of approx. $4\,\mathrm{m} \times 4.5\,\mathrm{m} \times 5\,\mathrm{m}$ open space and a relatively short measurement distance (0.23 m) were chosen.

The international standard IEC 1094-3 defines the free-field sensitivity product, $M_{f,a} \cdot M_{f,b}$ by the formula (A). A modification of this eliminates the transmitter current and leads to the applied formula (B).

$$M_{f,a} \cdot M_{f,b} = -j \cdot \frac{U_{R,b}}{I_{T,a}} \cdot \frac{2 d_{ab}}{\rho \cdot f} \cdot e^{\alpha d_{ab}} \qquad \text{(A)}$$

$$M_{f,a} \cdot M_{f,b} = -\frac{U_{R,b}}{U_{T,a}} \cdot \frac{d_{ab}}{\rho \cdot \pi \cdot f^2 \cdot C_a} \cdot e^{\alpha d_{ab}} \qquad \text{(B)}$$

$U_{R,b}$: Receiver output voltage
$U_{T,a}$: Transmitter driving voltage
d_{ab}: Distance between acoustic centres of the microphones
ρ: Air density
f: Frequency
C_a : Transmitter Capacitance
$\propto$: Sound attenuation of air

For all three pairs of microphones the output voltage of the receiver microphone, the voltage driving the transmitter and the transmitter capacitance

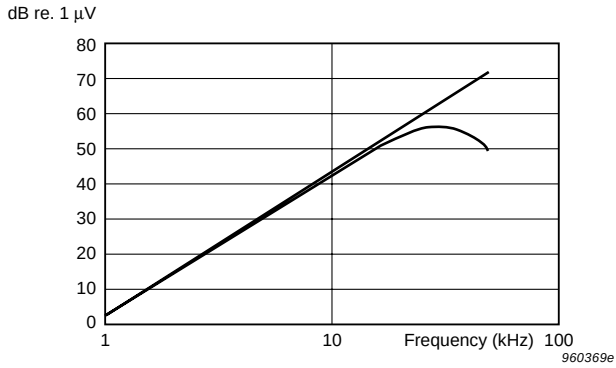

Fig. 2. Receiver Microphone Output Voltage as a function of frequency

were measured. During the measurement of the receiver voltage, the voltage across the transmitter was kept constant as a function of frequency. For flat microphone frequency responses this leads to a sound pressure and a receiver output which increase by 40 dB/decade and are very low at 1000 Hz where the measurements should preferably start; see Fig. 2.

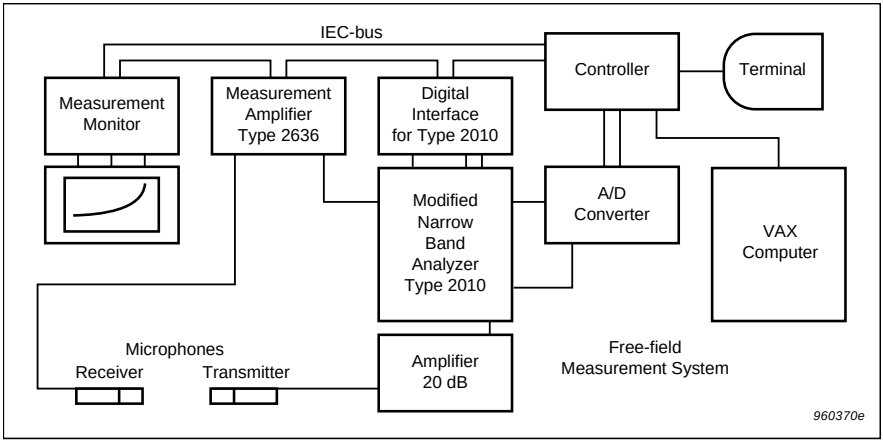

Fig. 3. Free-field Calibration System operating to 200 kHz. The possible accuracy is better than 0.025 dB at 0 dB SPL

To overcome problems with the signal to noise ratio Brüel & Kjær built a dedicated free-field calibration system some years ago. The system can work up to 200 kHz and thus cover the frequency range of most types of measurement microphones (sizes from 1″ to 1/8″). A block diagram of this system is shown in Fig. 3. The measurements were performed with this system at frequency steps of 100 Hz with a spread and a resolution better than 0.025 dB. Synchronous sampling and measurement times of up to half an hour at each of the lowest frequencies were used for improving the S/N-ratio.

After determination of the above parameters for the three pairs of microphones, the sensitivity products and the individual free-field sensitivity module were calculated using the formula below.

$$M_{f,a} = \left(\frac{U_{R,a} \cdot U_{R,c}}{U_{R,b}} \cdot \frac{U_{T,b}}{U_{T,a} \cdot U_{T,c}} \cdot \frac{d_{ab} \cdot d_{ca}}{d_{bc}} \cdot \frac{C_b}{C_a \cdot C_c} \cdot \frac{1}{\rho \cdot \pi \cdot f^2} \cdot e^{\alpha (d_{ab} - d_{bc} + d_{ca})} \right)^{\frac{1}{2}}$$

Electrostatic Actuator Response Calibration

The actuator responses were measured with 0.01 dB resolution and with the same measurement system as that used for the free-field measurements. This type of measurement is relatively easy to perform. The uncertainty of actuator calibration is high with respect to the absolute sensitivity. This is typically of the order 1 dB while it is very low for the frequency response calibration.

The response measured with an electrostatic actuator is generally influenced by the radiation impedance which loads the microphone diaphragm. For Type 4191, which has a relatively high diaphragm impedance, the influence ranges from essentially zero at low frequencies to about 0.3 dB at the highest frequencies (40 kHz). As the influence may be modified by the mechanical configuration of the actuator, the actuator type used for calibration service should be equal to that used for determination of the corrections.

Measured and Calculated Free-field Corrections

As mentioned above, the absolute sensitivity cannot be measured accurately with an electrostatic actuator. Therefore, there is no reason for also spending great efforts on obtaining an absolute measurement of the free-field response. The division of the free-field response by the actuator response will, anyway, give a result which contains a significant error. However, as this error makes a constant factor over the entire frequency range, some methods are available for its elimination.

From the laws of physics it can be concluded that the true corrections are small and gradually approaching zero dB at low frequencies. The resulting free-field correction may thus be determined visually from the shape of the measured and calculated curve which covers the frequency range from 1 kHz to 50 kHz. The accuracy obtained by this method is assumed to be significantly better than 0.1 dB. The curve shown in Fig. 4 gives the resulting free-field corrections determined by the above described method.

To verify the measured free-field correction results the microphone and the sound field were simulated by a mathematical model. The simulation accounted for the microphone dimensions, the diaphragm impedance and the properties of the ambient air. The simulation was made by Peter Juhl who also developed the applied boundary element model at the Acoustics Laboratory of

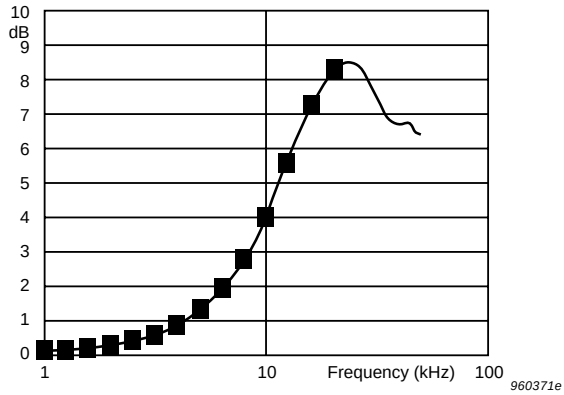

Fig. 4. Measured (curve) and calculated (points) free-field corrections for Type 4191 (0° incidence). The results are valid without protection grid. The calculated results support the measurement results

the Technical University in Lyngby, Denmark. The 1/3 octave calculation results are shown by the points in Fig. 4.

These results support the measurement results, especially at low frequencies while they are probably less reliable at the high frequencies due to lack of sufficient spatial resolution of the model.

Measurement of Directional Responses

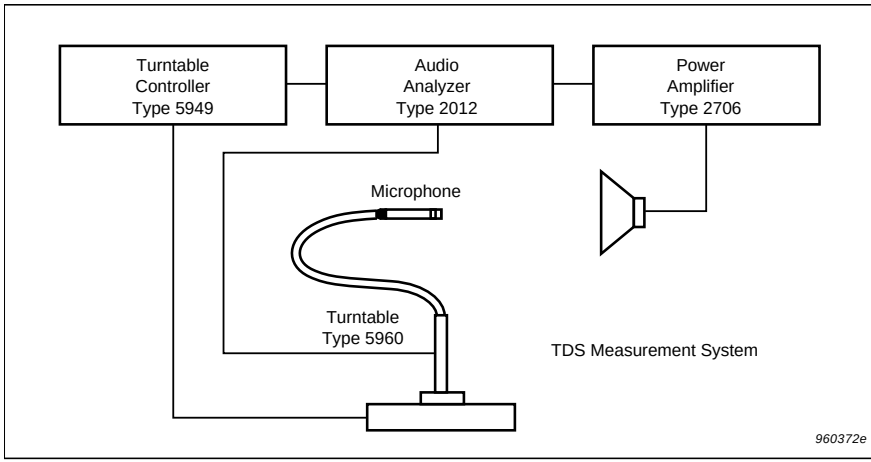

Fig. 5. The time selective measurement system for directional responses eliminates reflections

The free-field correction discussed above is valid for 0° incidence (reference direction). The sensitivities and corrections for other angles of incidence were determined relative to 0° for angle steps of 5° by the set-up shown in Fig. 5. The sound source was mounted in a fixed position while the receiving microphone was rotated to its different angles by an automatic turntable. The necessary, rather long, measurement distance and the turntable arrangement will generally lead to disturbing reflections. Therefore, a TDS measurement system based on the Brüel&Kjær Type 2012 was applied. This system makes time selective measurements and can eliminate reflections. The directional characteristics obtained are shown in Fig. 6.

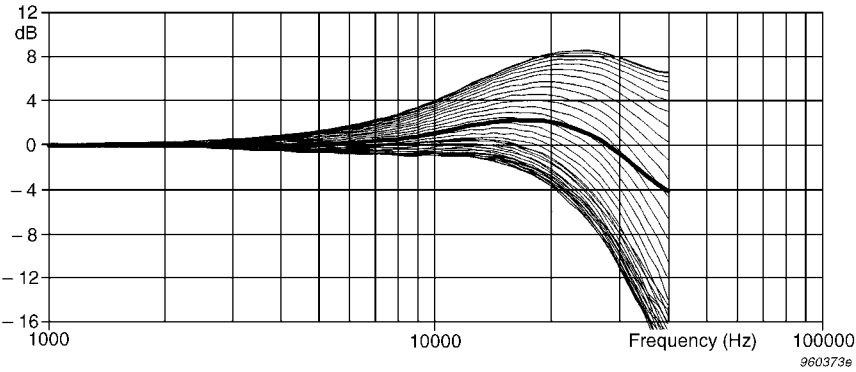

Fig. 6. Free-field corrections for Type 4191 without protection grid. The angles are stepped by 5 degrees

Random Incidence Corrections

The random incidence correction is calculated in accordance with the International Standard IEC 1183 (1994/95) which specifies how the calculation should be made. The free-field corrections shown in Fig. 6 were applied with weighting factors which account for that fraction of total power coming to the microphone from the specific directions. The resulting random incidence correction is also shown in Fig. 6.

Estimated Uncertainty of Free-field Corrections

The resulting uncertainties of the 0° free-field correction were estimated from the uncertainties of the parameters applied for its calculation. Their uncertainties were separated into groups of random and systematic errors as their weight in the reciprocity calculations are different. The systematic errors do partly eliminate each other while the non correlated or random errors add up statistically. The relative uncertainty of Free-field Response was determined by using the formula below:

$$\frac{\Delta M_f}{M_f} = A \cdot \left(\left(\frac{\Delta U_R}{U_R} \right)^2 + \left(\frac{\Delta U_T}{U_T} \right)^2 + \left(\frac{\Delta C}{C} \right)^2 + \left(\frac{\Delta f^2}{f^2} \right)^2 + \left(\frac{\Delta d}{d} \right)^2 + \left(\frac{\Delta \rho}{\rho} \right)^2 + \left(\alpha d \frac{\Delta \alpha}{\alpha} \right)^2 + \left(\alpha d \frac{\Delta d}{d} \right)^2 \right)^{\frac{1}{2}}$$

where the weighting factor 'A' equals 1/2 for the systematic and $\sqrt{3}/2$ for the random uncertainties respectively. After determination of other uncertainties related to the actuator response, the low frequency normalisation of the free-field corrections to 0 dB and to the influences of ambient pressure and temperature, the resulting uncertainty was calculated.

The uncertainty (tentative) of the free-field corrections for Type 4191 without grid was estimated to:

Frequency	1 kHz	2 kHz	4 kHz	8 kHz	16 kHz	32 kHz	40 kHz
Uncertainty ($2\times\sigma$)	0.03 dB	0.06 dB	0.08 dB	0.10 dB	0.12 dB	0.15 dB	0.20 dB

Notes:
The uncertainty (95% confidence level) is valid for the 0°-correction at 101.3 kPa, 23°C and 50% RH.

To calculate the uncertainty of a calibration for which the correction is applied, the uncertainty of the electrostatic actuator calibration must be taken into account. It should also be noted that the uncertainty of calibrations valid for microphones with protection grid are generally higher.

Conclusion

Free-field corrections were worked out for a new line of 1/2″ measurement microphones. The uncertainty of the Type 4191 free-field correction (0°-incidence) was analysed and calculated. The result agrees well with the uncertainty estimated from practical experience. The new corrections represent improvements in comparison with the corrections and the uncertainty estimated for earlier microphone types. The analysis revealed possibilities for further improvements in the future.

References

[1] IEC 486, *"Precision method for free-field calibration of one-inch standard condenser microphones by the reciprocity technique and the draft for the succeeding IEC document which includes 1/2" microphones*

[2] RASMUSSEN, K.: and SANDEMANN OLSEN, E.: *"Intercomparison on free-field calibration of microphones",* Final report (PL-07), the Acoustics Laboratory, Technical University of Denmark

[3] JUHL, P.: *"Numerical Investigation of Standard Condenser Microphones"* Journal of Sound and Vibration 1994 Vol. 177 (4) p. 433-446

Reduction of Non-linear Distortion in Condenser Microphones by Using Negative Load Capacitance

by Erling Frederiksen

Abstract

An analysis was made of the distortion produced by condenser measurement microphones which operate with stiffness controlled diaphragms. A calculation formula which was theoretically derived was verified by experiments. Analysis of this formula indicated that the distortion can be reduced by loading the microphone with a proper capacitance which has to be negative and is a function of the ratio between the backplate and diaphragm diameters. Experimental results confirmed this.

Résumé

Nous avons analys la distorsion produite par les microphones de mesure condensateur quips de diaphragmes dont la tension tait contrle. Une formule, rsultat dune approche thorique, indiquait que lon peut rduire le phnomne de distorsion en chargeant le microphone avec une capacit approprie, qui doit tre ngative et tenir compte du rapport entre les diamtres du diaphragme et de la plaque arrire. Cest ce quont confirm les expriences ralises.

Zusammenfassung

Es wurde die Verzerrung analysiert, die Kondensatormeßmikrofone aufweisen, wenn die Auslenkung der Membran durch ihre Steifigkeit bestimmt wird. Eine theoretisch abgeleitete Berechnungsformel wurde experimentell bestätigt. Die Analyse der Formeln wies darauf hin, daß sich die Verzerrung reduzieren läßt, wenn das Mikrofon mit einer geeigneten Kapazität belastet wird. Diese Kapazität ist negativ und eine Funktion des Quotienten aus den Durchmessern von Gegenelektrode und Membran. Das wurde durch Versuchsergebnisse bestätigt.

Introduction

Condenser measurement microphones have very wide dynamic ranges, typically 140 dB. At low sound levels the range is limited by inherent noise of the microphone and/or preamplifier. At high levels it is generally limited by nonlinear distortion which is proportional to the sound pressure and is produced by the microphone itself. This distortion has been analysed in theory and in practice for some frequently used types of microphones. The good agreement which was found between measured and calculated results verifies the derived distortion formulae and points clearly at the load capacitance and mode of diaphragm displacement as being the dominating reasons. The formulae were used for calculation of the capacitive loading which would lead to the lowest possible distortion. This appeared to be negative and to be a function of the ratio between the backplate and diaphragm diameters. Tests made with an experimental preamplifier with negative input capacitance gave promising results.

Theoretical Distortion Analysis of Transduction

General. The operation of most condenser measurement microphones is based on the application of a constant electrical charge stored on the active microphone capacitance and on its parallel (stray) capacitance. The constant charge may either be supplied from an external voltage source via a resistor (typically $10^9\,\Omega$) or by a built-in electret. The formulae below describe the transduction of capacitance variation to voltage:

$$E \cdot (C_a + C_p) = Q_0 = E_0 \cdot (C_0 + C_p) \quad or \quad E = E_0 \cdot \frac{C_0 + C_p}{C_a + C_p} \tag{1}$$

E : Voltage across capacitances with diaphragm displaced by sound pressure
E_0 : Voltage across capacitances with diaphragm at rest position
C_a : Active diaphragm-backplate capacitance (varies with sound pressure)
C_0 : Active diaphragm-backplate capacitance with diaphragm at rest position
C_p : Parallel capacitance (passive)
Q_0 : Constant charge stored on the active and passive capacitances

As the charge (Q_0) is kept constant the voltage (E) will vary with the variation of the active capacitance (C_a) which is caused by the sound pressure. The voltage produced depends on the microphone configuration and on the diaphragm deflection mode.

Flat Diaphragm Displacement Mode

If the microphone diaphragm is considered to be parallel to a circular backplate and displaced like a flat piston, then the active capacitance (C_a) and its rest capacitance (C_0) can be expressed by the equations:

$$C_a = R_s \cdot \frac{\varepsilon \cdot \pi \cdot R_b^2}{D+d} = C_0 \cdot (1+y)^{-1}$$

$$C_0 = R_s \cdot \frac{\varepsilon \cdot \pi \cdot R_b^2}{D} \qquad \text{where } R_s = \frac{A_b - A_h}{A_b} \quad \text{and} \quad y = \frac{d}{D}$$

ε : Dielectric constant of air
R_b : Radius of backplate
D : Rest distance, backplate to diaphragm
d : Displacement of diaphragm
R_s : Ratio of effective and total backplate area
A_b : Total backplate area (includes area of holes)
A_h : Area of holes in backplate (a uniform hole distribution is considered)
y : Relative diaphragm displacement

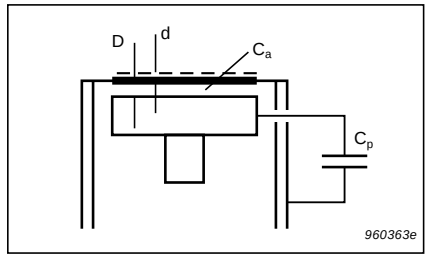

Fig. 1. Microphone with flat diaphragm displacement mode and parallel capacitance

Insertion of the above expressions into Equation (1) leads to Equation (2) which defines the output voltage of a microphone with a flat diaphragm displacement mode:

$$E_{fm} = E_0 \cdot \frac{C_0 + C_p}{C_0 \cdot (1+y)^{-1} + C_p} \tag{2}$$

Series expansion of equation (2) leads to:

$$E_{fm} = E_0 + E_0 \cdot \frac{C_0}{C_0 + C_p} \cdot \left(y - \left(\frac{C_p}{C_0 + C_p} \right)^1 \cdot y^2 + \left(\frac{C_p}{C_0 + C_p} \right)^2 \cdot y^3 - ..... \right) \tag{2a}$$

For a sinusoidally varying diaphragm displacement with time y, y^2 and y^3 become:

$$y = y_m \cdot \sin \omega t;\ y^2 = \frac{1}{2} \cdot y_m^2 \cdot (1 - \cos 2\omega t);\ y^3 = \frac{1}{4} \cdot y_m^3 \cdot (3 \sin \omega t - \sin 3\omega t)$$

where y_m : Maximum value of relative diaphragm displacement.

This leads to the following second (D_2) and third (D_3) harmonic distortion components of the output voltage (relative to the fundamental frequency component):

$$D_2 = \left(\frac{1}{2} \cdot y_m \cdot \frac{C_p}{C_0 + C_p} \right)^1 \cdot 100\% \text{ and } D_3 = \left(\frac{1}{2} \cdot y_m \cdot \frac{C_p}{C_0 + C_p} \right)^2 \cdot 100\%$$

The dominating second harmonic component (D_2) is proportional to the diaphragm displacement and thus to the sound pressure while the third harmonic (D_3) is proportional to the square of the pressure. Notice, that the distortion decreases with the parallel capacitance and that it becomes zero if this capacitance becomes zero ($C_p = 0$).

Parabolic Diaphragm Displacement Mode

Generally condenser microphones use foil diaphragms with a high internal mechanical tension which gives the diaphragm its required stiffness and determines the displacement mode at lower frequencies. At higher frequencies the air damping and the foil mass do also influence the mode. This discussion covers only the low frequency mode which can be considered to occur up to a frequency which is 0.2 to 0.5 times the diaphragm resonance frequency. The displacement mode of an ideal circular diaphragm, which is purely stiffness controlled, is defined by the formula below and illustrated in Fig. 2:

$$d(r) = d_0 \cdot \left(1 - \frac{r^2}{R_d^2}\right)$$

where

d_0 : centre displacement
r : distance to centre
R_d : Radius of diaphragm

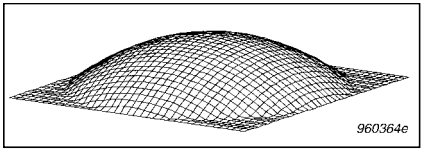

Fig. 2. Calculated foil diaphragm displacement mode

To verify this the displacement mode of a one inch microphone Type 4144 was measured. This was done by scanning its diaphragm along a diameter. The scanning was made with a small microphone (Type 4138, 1.8 mm backplate diameter) with its own diaphragm dismantled. This microphone was moved at a fixed distance in front of the large diaphragm in such a way that it detected the local displacement of the larger diaphragm while this was exposed to sound pressure. The measured and the calculated displacement magnitude were found to be in very good agreement; see Fig. 3.

Considering the above displacement mode the active capacitance (C_a) and its rest capacitance (C_0) may be expressed by the equations below:

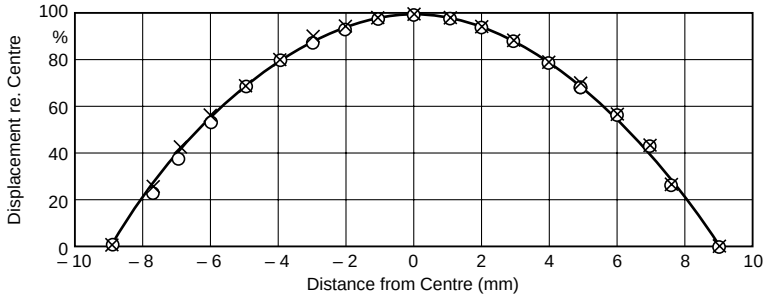

Fig. 3. Diaphragm displacement as a function of distance to centre for a one inch microphone with a diaphragm of 18 mm diameter. The points are measured at 40 Hz and at 130 dB and 150 dB SPL. The curve is calculated

$$C_a = R_s \cdot \int_0^{R_b} \frac{\varepsilon \cdot 2 \cdot \pi \cdot r}{D + d_0 \cdot \left(1 - \frac{r^2}{R_d^2}\right)} \, dr \qquad C_0 = R_s \cdot \frac{\varepsilon \cdot \pi \cdot R_b^2}{D}$$

where $R_s = \frac{A_b - A_h}{A_b}$

Simplification and integration of the above equation leads to:

$$C_a = R_s \cdot \frac{\varepsilon \cdot \pi \cdot R_b^2}{D} \cdot R_b^{-2} \cdot \int_0^{R_b} \frac{2 \cdot r}{1 + y_0 \cdot \left(1 - \frac{r^2}{R_d^2}\right)} \, dr$$

$$C_a = C_0 \cdot R_b^{-2} \cdot \int_0^{R_b} \frac{2 \cdot r}{1 + y_0 \cdot \left(1 - \frac{r^2}{R_d^2}\right)} dr$$

$$C_a = C_o \cdot \left(\frac{R_b^2}{R_d^2}\right)^{-1} \cdot y_0^{-1} \cdot \ln \frac{1 + y_0}{1 + \left(1 - \frac{R_b^2}{R_d^2}\right) \cdot y_0}$$

$$C_a = C_0 \cdot (1-k)^{-1} \cdot y_0^{-1} \cdot \ln \frac{1 + y_0}{1 + k \cdot y_0}$$

where $k = 1 - \frac{R_b^2}{R_d^2}$ and $y_0 = \frac{d_0}{D}$

Insertion of C_a and C_0 in Equation (1) gives the equation valid for parabolic mode:

$$E_{pm} = E_0 \cdot \frac{C_0 + C_p}{C_0 \cdot (1-k)^{-1} \cdot y_0^{-1} \cdot \ln \frac{1 + y_0}{1 + k \cdot y_0} + C_p} \tag{3}$$

Series expansion of Equation (3) leads to:

$$E_{pm} = E_0 + E_0 \cdot \frac{k+1}{2} \cdot \frac{C_0}{C_0 + C_p} \cdot (y_0 + F_2 \cdot y_0^2 + F_3 \cdot y_0^3 + \ldots.) \tag{3a}$$

where

$$F_2 = -\frac{C_0 \cdot (k^2 - 2 \cdot k + 1) + 4 \cdot C_p \cdot (k^2 + k + 1)}{6 \cdot (C_0 + C_p) \cdot (k + 1)} \quad \text{and}$$

$$F_3 = \frac{(C_0^2 + 4 \cdot C_0 \cdot C_p) \cdot (k^2 - 2 \cdot k + 1) + 6 \cdot C_p^2 \cdot (k^2 + 1)}{12 \cdot (C_0 + C_p)^2}$$

The factors F_2 and F_3 are functions of the parameter k and thus of the ratio between the backplate and diaphragm radii. The larger the backplate becomes, the higher becomes the distortion. Equation (2a) indicates that this effect was to be expected as area added along the outer circumference represents a less active capacitance which loads the more active capacitance located at the diaphragm and backplate centres.

Notice, that the smaller the backplate becomes in comparison with the diaphragm, the more flat does the active part of the diaphragm becomes. Therefore, for k equal to '1', Equation (3a) becomes equal to Equation (2a) which is valid for flat diaphragm mode. In practice, distortion should be defined as a function of Sound Pressure (p) rather than relative diaphragm displacement at the centre (y_0). The relation between displacement and sound pressure can be obtained from the following equations:

$$e_1 = E_0 \cdot \frac{k+1}{2} \cdot \frac{C_0}{C_0 + C_p} \cdot y_0 \quad \text{and} \quad p = e_1 \cdot \left(S_0 \cdot \frac{C_0 + C_p - C_i}{C_0 + C_p} \right)^{-1}$$

e_1 : Microphone output voltage according to Equation (3a) (1st term with y_0)
p : Sound pressure
S_0 : Measured open circuit sensitivity

For a sinusoidal diaphragm displacement with time, the ratios (D_2 and D_3) between the second and third harmonic components and the fundamental component become:

$$D_2 = \left(\frac{y_m}{2}\right)^1 \cdot F_2 \cdot 100\% \tag{4}$$

and

$$D_3 = \left(\frac{y_m}{2}\right)^2 \cdot F_3 \cdot 100\% \tag{5}$$

where $y_m = \sqrt{2} \cdot p_{RMS} \cdot \frac{S_0}{E_0} \cdot \frac{C_0 + C_p - C_i}{C_0} \cdot \frac{2}{k+1}$

Comparison of Calculated and Measured Distortion

Calculated and measured distortion data were evaluated by comparison. See input data and distortion results for some commonly used microphones in the tables below.

B&K Type No.		4144	4133	4165	4135	4190	4192/93
Dimension		1/1″	1/2″	1/2″	1/4″	1/2″	1/2″
S_0	mV/Pa	50	12	50	4.0	50	12.5
E_0	V	200	200	200	200	200	200
R_d	mm	9.1	4.6	4.6	2.1	4.6	4.6
R_b	mm	6.65	3.60	3.65	1.75	3.45	3.45
D_0	µm	23.5	21.0	22.2	18.0	24.5	19.0
A_h	mm^2	20.3	1.70	4.24	0	3.96	5.50
C_e	pF	2.1	0.5	0.9	0.2	0.8	0.8
C_h	pF	2.1	1.1	1.8	1.6	1.6	1.5

B&K Type No.		**4144**	**4133**	**4165**	**4135**	**4190**	**4192**	**4193**
Load Capacitance	pF	0.2	0.2	0.2	0.2	0.2	0.2	100
Sound Pressure Level	dB	140	150	140	160	140	150	150
2. harm. calculated	%	0.51	0.49	0.97	1.52	0.97	0.63	3.0
2. harm. measured *	%	0.56	0.50	1.08	1.55	0.90	0.54	3.4
Ratio - Calc. re. HB-data		**0.91**	**0.97**	**0.98**	**0.98**	**1.08**	**1.17**	**0.88**
3. harm. calculated	%	0.01	0.01	0.02	0.04	0.02	0.01	0.09

* Sources: Brüel & Kjær's blue Microphone Handbook and the Falcon Handbook. The data applied for Types 4133 and 4165 originates from measurements performed in January 1994

There is very good agreement between the calculated and the measured distortion data. The calculated ratio (see lower table) is very close to one. As the calculations only account for the transduction itself this seems to be the only source of low frequency distortion which is of importance for the analysed types of microphones.

Distortion Reduction By Negative Capacitance Loading

Theory

Equation (4) shows that the 2nd harmonic component is proportional to the factor F_2. It is a function of the ratio between the active and the passive parallel capacitances as well as of the ratio between the backplate and diaphragm radii. For a certain radii ratio (i.e. a certain value of '*k*') F_2 and the second harmonic distortion become zero if the microphone is loaded with a proper negative capacitance. Calculated distortion is shown for two extreme microphone configurations in Fig.4.

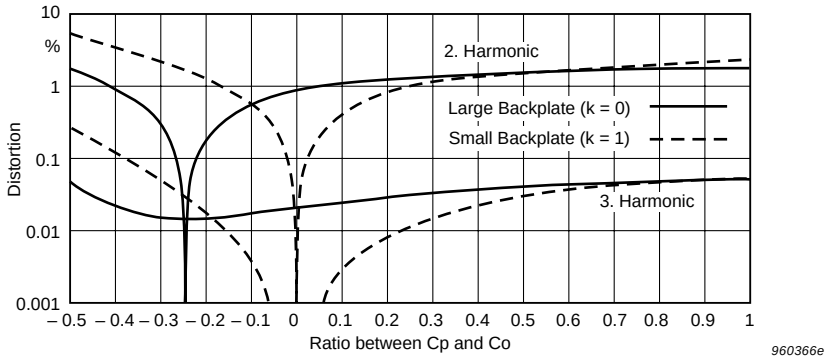

Fig. 4. Harmonic distortion calculated as a function of the ratio between the passive and active capacitances

Typical microphone/preamplifier combinations have a C_p/C_0-ratio of + 0.1 to + 0.4. Fig. 4 shows that the optimum with respect to distortion is between '– 0.25' and '0'. The ideal C_p/C_0-ratio is defined by the following equation:

$$\left(\frac{C_p}{C_0}\right)_{ideal} = -\frac{1}{4} \cdot \frac{k^2 - 2 \cdot k + 1}{k^2 + k + 1}$$

Negative Capacitance

In principle, negative load capacitance may be created by a circuit like that shown in Fig. 5. A capacitor (C) is connected between the input and output of the microphone preamplifier whose gain (>+1) can be adjusted to give the proper input capacitance (C_i); see the formula:

$$C_i = \frac{e_1 - e_2}{e_1} \cdot C = (1 - A) \cdot C$$

where e_1: input voltage, e_2: output voltage

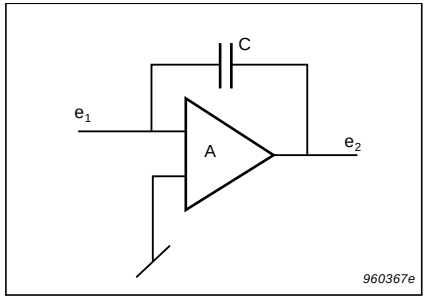

Fig. 5. Principle of negative input capacitance circuit

Experimental Results

An experimental preamplifier with adjustable negative input capacitance was designed and tested with three different microphones at 100 Hz. For each microphone the capacitance was adjusted to give the lowest possible 2nd harmonic distortion. The results are shown in the table below:

Initial Experimental Results obtained with Negative Input Capacitance	Unit	Type 4165	Type 4133	Type 4135
Sound Pressure Level	dB	134	146	156
Nominal 2. harmonic distortion	%	0.61	0.32	0.98
Minimised 2. harmonic distortion (negative cap.)	%	0.10	0.16	0.18
Reduction factor	**–**	**6.1**	**2.0**	**5.4**
Measured increase of sensitivity (approximate)	dB	2.0	1.5	4.3
Calculated increase of sensitivity	dB	2.0	1.4	3.6
Optimal input capacitance (calculated)	pF	–3.7	–2.6	–2.2

The idea (patented) of using negative input capacitance for distortion reduction seems to work well in practice but further experiments have to be made to clarify all aspects of its use. The Brüel & Kjær High Pressure Calibrator Type 4221 was used for the distortion measurements.

Conclusion

Harmonic distortion of condenser microphones using constant electrical charge has been analysed for the frequency range where the diaphragm displacement is stiffness controlled. Distortion formulae have been derived for the transduction from diaphragm displacement to output voltage. The formulae were applied for calculating distortion of some commonly applied types of measurement microphones. The results were compared with data supplied by the manufacturer and very good agreement was found. This verified the formulae and pointed at parallel capacitance and displacement mode as being the dominating reason for the distortion. The distortion analysis indicated the possibility of reducing harmonic distortion by loading the microphone with negative capacitance. This was confirmed by experiments.

Further work has to be done to analyse the practical possibilities which in addition to distortion reduction might be improvement of high level peak measurements and extension of the applicable dynamic range of condenser microphones.

In Situ Verification of Accelerometer Function And Mounting

by Torben R. Licht

Abstract

Piezoelectric accelerometers are used for vibration measurements in a huge variety of measurement situations. Many different ways of checking the integrity of a measurement channel have been devised, from tapping on the structure to very sophisticated measurement schemes such as complex impedance measurements. A new practical charge amplifier input system which permits in situ check of accelerometer functionality and mounting performance has been developed. (Patent pending). A description of the system and performance examples will be given.

Résumé

Les accéléromètres piézoélectriques interviennent dans de nombreux types de mesures vibratoires. De nombreuses méthodes de vérification de l'intégrité de la chaîne de mesure ont été mises en œuvre, des simples impacts sur la structure jusqu'à des dispositifs de mesure d'impédance complexe. Un nouveau système d'entrée d'amplification de charge très pratique vient d'être mis au point pour permettre la vérification in situ des fonctionnalités de l'accéléromètre et des performances de l'installation (en instance de brevet). Il est décrit dans ces pages et ses performances sont illustrées par des exemples.

Zusammenfassung

Piezoelektrische Beschleunigungsmesser werden für eine Vielzahl von Schwingungsmessungen verwendet. Um die Integrität des Meßkanals zu prüfen, wurden zahlreiche Methoden entwickelt, vom Beklopfen der Struktur bis zu hochkomplizierten Meßverfahren wie die Messung der komplexen Impedanz. Es wurde ein neues praktisches Ladungsverstärker-Eingangssystem entwickelt, mit dem sich Funktionstüchtigkeit und Befestigung von Beschleunigungsaufnehmern in situ prüfen lassen. (Patent angemeldet). Es folgen eine Beschreibung des Systems und Beispiele für seine Leistungsfähigkeit.

Introduction

Piezoelectric accelerometers are used extensively to measure vibration on many different structures and with many different vibration sources.

A number of different techniques are used to ensure the proper functioning of each measurement channel, but only a few very complicated methods have been used to verify the mechanical integrity of the transducer and its mounting.

This is even more serious because the handling and mounting are often carried out by people without knowledge of vibration measurement techniques.

Both statistics and an educated guess indicate that, on a list of common problems with piezoelectric accelerometers, the first is cabling and the second is mounting.

Therefore it is believed that the simple method for testing mounted transducers, described in the following, can make a significant contribution to the quality of future vibration measurements.

Accelerometer Theory

Normally an accelerometer is described as a seismic transducer with the simple model shown below. k is the stiffness of the spring, c the damping and m the seismic mass.

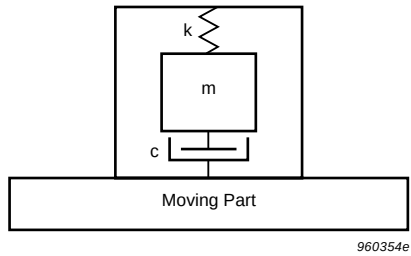

Fig. 1

The ratio between the motion amplitude of the moving part and the relative motion of the mass with respect to the housing can be described in magnitude and phase by the formulae

$$R_d = \frac{\left(\frac{\omega}{\omega_r}\right)^2}{\sqrt{\left[1-\left(\frac{\omega}{\omega_r}\right)^2\right]^2 + \left[2d\frac{\omega}{\omega_r}\right]^2}} \quad \text{and} \quad \theta = \tan^{-1}\frac{2d\frac{\omega}{\omega_r}}{1-\left(\frac{\omega}{\omega_r}\right)^2}$$

where $d=c/c_c$ is the fraction of critical damping $(c_c = 2\sqrt{km} = 2m\omega_r)$ and $\omega_r = \sqrt{\frac{k}{m}}$ is the resonant angular frequency.

For accelerometers the input is taken as acceleration of the moving part yielding $R_a=-R_d/\omega^2$. The resulting general curves are shown here.

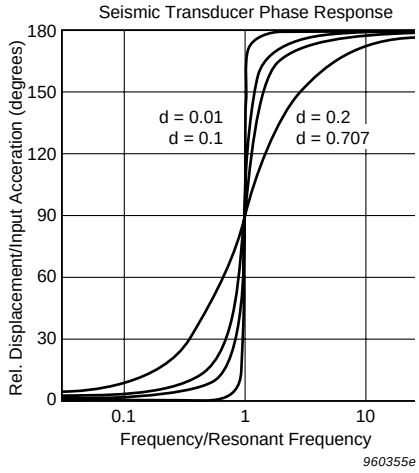

Fig. 2

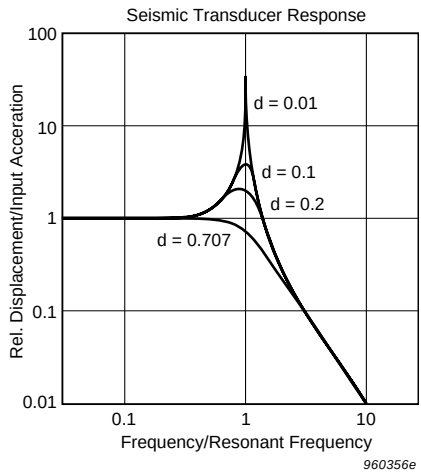

Fig. 3

Practically all piezoelectric accelerometers have a negligible damping in the order of 0.01, which means that the resonance peak has a high Quality Factor Q, making it possible to excite the resonance and observe the decaying signal. To include the mounting, the model has to be extended to the following where the base and mounting stiffness is included as separate items and the damping has been omitted.

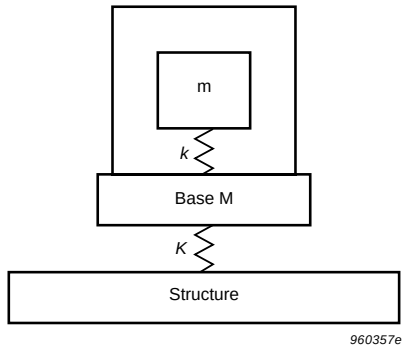

Fig. 4

The normal modes of such a system is described by the roots of the equation

$$\begin{vmatrix} M\omega^2 - (k+K) & k \\ k & m\omega^2 - k \end{vmatrix} = 0 \quad \text{or}$$

$$Mm\omega^4 - (m\ (k+K) + Mk\ )\omega^2 + kK = 0 \quad \text{giving the roots}$$

$$\omega^2 = \omega_m^2 \left[1 + \frac{R}{2} \pm \sqrt{1 + \left(\frac{R}{2}\right)^2} \right]$$

where $R = K/k$ is the ratio between the two spring constants and $\omega_m = \sqrt{\frac{k}{m}}$ is the mounted resonance frequency.

The two modes described by the formula are shown in the graph below.

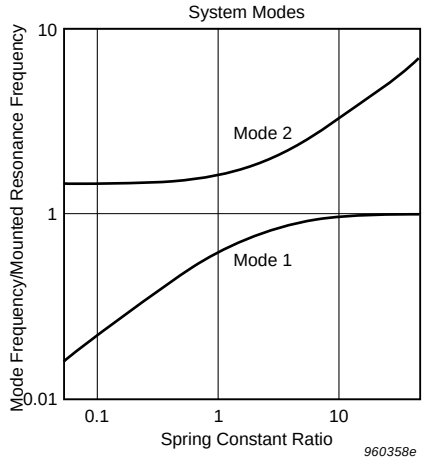

Fig. 5

Test Method

The basic idea of the test method is based on the reciprocal nature of the piezoelectric material, i.e. if a voltage is applied to the piezoelectric discs they will change shape, following the general equation

$$\Delta x = d_{xy} \cdot V$$

where d_{xy} is the appropriate piezoelectric constant, mostly d_{33} (compression constructions) or d_{15} (shear constructions).

This implies that on transducer designs with low damping and relatively high coupling (high d) an electrical pulse can be used to excite the structure and make it "ring" or vibrate at its resonance frequency for an extended period of time.

The decrease in amplitude is given by the logarithmic decrement

$$\Delta \approx 2\pi d$$

which for a damping $d = 0.01$ gives $\Delta = 0.06$ i.e. the amplitude decreases 6% per oscillation, leaving a number of oscillations in the order of 50 to be observed.

The frequency observed will be the dominant mode of the two shown above. A well mounted accelerometer, i.e. where a high spring constant ratio is obtained, will then resonate at the mounted resonance frequency. However, the more loose the mounting becomes, the lower will that mode frequency be and the more the free hanging resonance will become dominant. This gives 1.4 times the mounted resonance in the typical case shown in the figure.

The amplitude of the signal can be used as a check on the accelerometer sensitivity squared.

Implementation

In the Brüel & Kjær Measuring Amplifier Type 2525 a function has been implemented to exploit the idea described previously.

The instrument contains a generator which can generate a single square pulse, as well as the logical circuitry to switch the generator in and out in front of the charge amplifier. The time signal is shown schematically below.

A counter with gating is also included in the amplifier. This permits the direct display of the measured resonance frequency of the system tested.

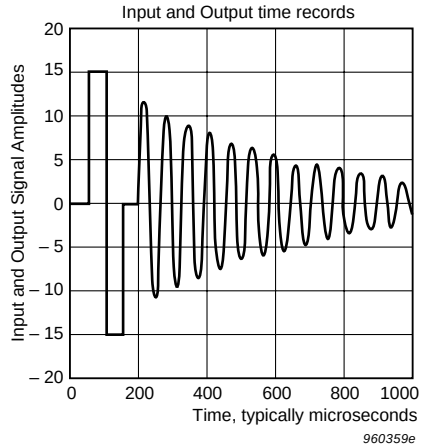

Fig. 6

Examples of Application

An accelerometer Type 4382 with a specified mounted resonance frequency of 28 kHz ± 10% and a mass of 17 grams was mounted on a large steel block. A good, smooth surface was present at the mounting position.

The measured resonance frequency as a function of the mounting torque was measured. The results are shown in Table 1.

Mounting torque [Nm]	Resonance frequeny [kHz]
0.4	25.76
0.8	26.87
1.2	26.87
1.6	26.87
2.0	26.87

Table 1. Dependence of resonance frequency on mounting torque

The results show that when a good mounting surface is made the torque is not critical for low level measurements (at higher vibration levels the transducer might lose contact to the surface with dramatic errors as a result).

To simulate a bad surface a single 0.18 mm (0.007″) strand of copper wire was introduced between the accelerometer and the mounting surface. A frequency of 21.28 kHz was measured, which shows the dramatic change from 26,87 to 21.28 kHz on the resonance.

Another experiment was made to show the kind of information which can be obtained.

A plate has a certain local stiffness, i.e. in principle, a certain mechanical impedance. When we mount an accelerometer of a certain mass M, i.e. a certain mechanical impedance equal to jωM, we load the plate and change its parameters, e.g. the resonance frequencies according to the ratio between the two impedances.

If the plate impedance is large compared to the accelerometer impedance this will also mean that the accelerometer mounted resonance will be close to the specified typical value. Whereas if the plate is thin and has an impedance which is low compared to that of the accelerometer, the mounted resonance found will tend to approach the free hanging frequency. This will indicate that we have introduced important changes to the structure.

A number of measurements were made on steel plates with thicknesses from 1 to 10 mm (0.04 to 0.4″). The results are shown in Table 2.

It is seen that the accelerometer starts to affect the vibration even at relatively large plate thicknesses.

Plate Thickness [mm]	Measured Resonance Frequency [kHz]
1.0	36.96
1.5	34.72
2.0	33.60
3.0	31.36
10.0	29.11

Table 2. Resonance frequency as function of plate thickness

Other Ways To Implement This Method

When using frequency analyzers more information can be obtained. If the 2525 is used, the output signal can be analysed even when resonances are not pronounced and several different frequencies may be observed.

When using advanced FFT (Fast Fourier Transform) analyzers containing special generators like the Brüel&Kjær Type 3550, other possibilities exist. A transformer can be inserted between the accelerometer and the charge amplifier input. This allows a pulse to be injected into the system using the generator.

The system is shown schematically below.

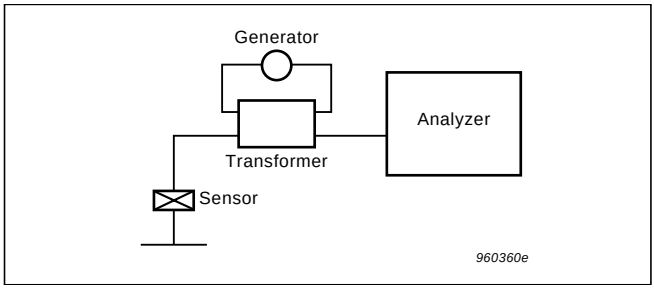

Fig. 7

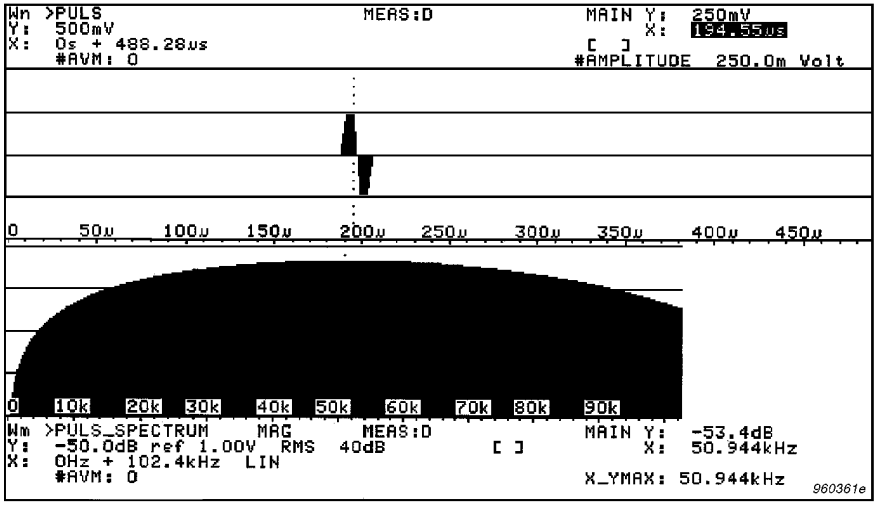

Fig. 8 The pulse used for testing and its spectrum on a 40 dB display range

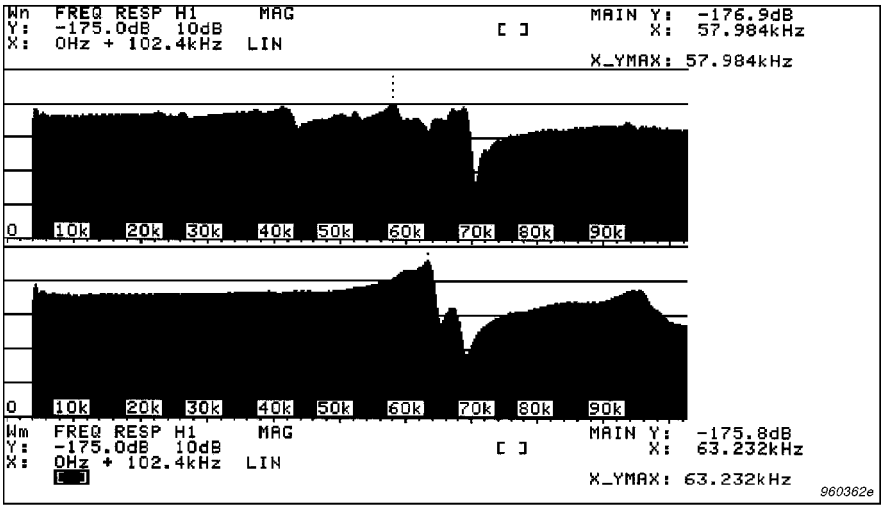

Fig. 9 Knock transducer measured mounted (upper) and unmounted (lower)

The generator signal, its frequency content and the response from a mounted and unmounted knock sensor is shown in Figs. 8 and 9.

The pulse applied has the important properties of no frequency content at DC and a broad continuous spectrum. This is similar to the pulse produced by built-in generator of the Measuring Amplifier Type 2525.

The unmounted response shows a first resonance at 63 kHz and some more resonances at higher frequencies.

The mounted response shows a rather complicated response (in contrast to most accelerometers) with the most pronounced resonance at 58 kHz.

It is seen that a lot of information can be obtained from FFT analysis. In particular, it is believed to be a viable method for quality control of transducers made in large numbers, like the knock sensors shown here.

Conclusion

A new, simple method for checking the performance of piezoelectric transducers has been described.

A simple instrument implementing this method has been tested and the results showed good agreement with the theory.

An advanced FFT analyzer has been demonstrated to be able to exploit the method even further.

It is believed that this method can help the vibration measuring community to improve the total quality of its work in the future.

References

[1] HARRIS & CREDE: *"Shock and Vibration Handbook"*, McGraw-Hill, Inc., 1976

[2] SERRIDGE, M. & LICHT T.: *"Piezoelectric Accelerometers and Preamplifiers"*, Brüel & Kjær, 1987

[3] Measuring Amplifier Type 2525, Instruction Manual, Brüel & Kjær, 1994

[4] WISMER, N.J. and KONSTANTIN-HANSEN, H.: "*Mounted Resonance Measurements using Type 2525"*. Application Note, BO 0413, Brüel & Kjær, 1994

Previously issued numbers of Brüel & Kjær Technical Review

(Continued from cover page 2)

1 – 1986 Environmental Noise Measurements
4 – 1985 Validity of Intensity Measurements in Partially Diffuse Sound Field
Influence of Tripods and Microphone Clips on the Frequency Response of Microphones
3 – 1985 The Modulation Transfer Function in Room Acoustics
RASTI: A Tool for Evaluating Auditoria
2 – 1985 Heat Stress
A New Thermal Anemometer Probe for Indoor Air Velocity Measurements
1 – 1985 Local Thermal Discomfort
4 – 1984 Methods for the Calculation of Contrast
Proper Use of Weighting Functions for Impact Testing
Computer Data Acquisition from Brüel & Kjær Digital Frequency Analyzers 2131/2134 Using their Memory as a Buffer
3 – 1984 The Hilbert Transform
Microphone System for Extremely Low Sound Levels
Averaging Times of Level Recorder 2317
2 – 1984 Dual Channel FFT Analysis (Part II)
1 – 1984 Dual Channel FFT Analysis (Part I)
4 – 1983 Sound Level Meters — The Atlantic Divide
Design Principles for Integrating Sound Level Meters
3 – 1983 Fourier Analysis of Surface Roughness
2 – 1983 System Analysis and Time Delay Spectrometry (Part II)

Special technical literature

Brüel & Kjær publishes a variety of technical literature which can be obtained from your local Brüel & Kjær representative.
The following literature is presently available:

- Modal Analysis of Large Structures – Multiple Exciter Systems (English)
- Acoustic Noise Measurements (English), 5th. Edition
- Noise Control (English, French)
- Frequency Analysis (English), 3rd. Edition
- Catalogues (several languages)
- Product Data Sheets (English, German, French, Russian)

Furthermore, back copies of the Technical Review can be supplied as shown in the list above. Older issues may be obtained provided they are still in stock.

WORLD HEADQUARTERS: DK-2850 Nærum · Denmark
Telephone: +45 42 80 05 00 · Fax: +45 42 80 14 05 · e-mail: info@bk.dk

Australia (02) 246-0266 · Austria 0043-1-865 74 00 · Belgium 016/44 22 25 · Brazil (011) 246-3166
Canada: (514) 695-8225 · China 10654 12 635 / 10 654 37 495 · Czech Republic 02-67021100 · Finland 90-223 3021
France (1) 69 20 63 00 · Germany 0561/8 142-0 · Holland (0)3 05 69 22 24 · Hong Kong 25 48 74 86
Hungary (1) 215 83 05 · Italy (02) 57 60 41 41 · Japan 03-3779-3671 · Republic of Korea (02) 3473-0605
Norway 66 90 44 10 · Poland (0-22) 40 23 62 · Portugal (1) 471 14 63 · Singapore (65) 275-35 15
Slovak Republic 07-37 61 31 · Spain (91) 368 10 00 · Sweden (08) 711 27 30 · Switzerland 01/940 03 03
Taiwan (02) 713 9303 · United Kingdom and Ireland (0181) 954-2366 · USA (800) 332-2040
Local representatives and service organisations worldwide

ISSN 007 – 2621
BV 0048 – 11